Mineralogical Magazine, February 2017, Vol. 81(1), pp. 167–173

A multimethodic approach for the characterization of manganiceladonite, a new member of the celadonite family from Cerchiara mine, Eastern Liguria, Italy

G. O. Lepore[1,*], L. Bindi[1], F. Di Benedetto[1], E. Mugnaioli[2,3], C. Viti[2], A. Zanetti[4], M. E. Ciriotti[5] and P. Bonazzi[1]

[1] Dipartimento di Scienze della Terra, Università degli Studi di Firenze, Via G. La Pira 4, I-50121, Firenze, Italy
[2] Dipartimento di Scienze Fisiche, della Terra e dell'Ambiente, Università di Siena, Via Laterina 8, I-53100, Siena, Italy
[3] Center for Nanotechnology Innovation@NEST, Istituto Italiano di Tecnologia, Piazza San Silvestro 12, 56127, Pisa, Italy
[4] CNR, Istituto di Geoscienze e Georisorse, Università di Pavia, Via Ferrata 1, I-27100 Pavia, Italy
[5] Associazione Micromineralogica Italiana, Via Gioconda 3, I-26100 Cremona, Italy

[*Received 1 December 2015; Accepted 31 January 2016; Associate Editor: Sergey Krivovichev*]

ABSTRACT

In the manganesiferous ores associated with the metacherts of the ophiolitic sequences at the Cerchiara mine, Eastern Liguria (Italy), a new Mn-bearing mineral belonging to the mica group has been recently found and characterized. High resolution transmission electron microscopy and electron diffraction tomography studies confirm that the mineral belongs to the mica group. Unit-cell parameters from the powder diffraction pattern are: $a = 5.149(1)$, $b = 8.915(1)$, $c = 10.304(1)$ Å, $\beta = 102.03(1)°$, space group $C2$ or $C2/m$. On the basis of the electron paramagnetic resonance spectroscopic results, the Mn^{4+} content represents a very subordinate fraction of the total Mn, the remaining occurring as Mn^{3+}. The Raman spectrum clearly indicates the presence of OH groups in the structure. Laser-ablation inductively-coupled-plasma mass-spectrometry measurements assess the presence of considerable amounts of Li.

Assuming all Mn as Mn^{3+} and 22 negative charges, the empirical formula can be expressed as: $(K_{0.83}\square_{0.17})(Mn^{3+}_{1.14}Mg_{0.80}Li_{0.20}Fe^{3+}_{0.02})(Si_{3.89}Al_{0.10})O_{10}[(OH)_{1.92}F_{0.08}]$ with the sum of the octahedral cations indicating a 'transitional' character between a di- and a tri-octahedral structure. This formula corresponds ideally to the Mn^{3+} analogue of celadonite, thus expanding the range of solid solution in the celadonite family. The ideal end-member formula $KMn^{3+}MgSi_4O_{10}(OH)_2$ can be easily related to celadonite by the homovalent substitution $^{VI}Mn^{3+} \rightarrow {}^{VI}Fe^{3+}$. The mineral and its name have been approved by the Commission on New Minerals, Nomenclature and Classification of the International Mineralogical Association, (IMA 2015-052).

Keywords: manganiceladonite, celadonite family, Cerchiara mine, Eastern Liguria, Italy.

Introduction

High concentrations of Mn in the mica-group minerals are quite rare, although several Mn-bearing micas do actually exist. The $Mn^{2+} \rightarrow Fe^{2+}$ substitution relates shirozulite (Ishida *et al*., 2004) to annite, as well as masutomilite (Harada *et al*., 1976) to 'zinnwaldite'. Norrishite (Eggleton and Ashley, 1989; Tyrna and Guggenheim, 1991) is a trioctahedral mica with the M2 site occupied mainly by Mn^{3+} and M1 by Li. Hendricksite, polylithionite and kinoshitalite have been reported to bear significantly large amounts of Mn (Guggenheim *et al*., 1983; Boggs, 1992; Tracy

*E-mail: lepore@esrf.fr
https://doi.org/10.1180/minmag.2016.080.087

and Beard, 2003, respectively). Montdorite (Robert and Maury, 1979) is an uncommon Mn-bearing, tetrasilicic transitional mica with Mn content up to ~0.7 atoms per formula unit (apfu). However, it is rare for these minerals to reach the ideal end-member composition (Tischendorf *et al*., 2007). Preliminary chemical analyses obtained by energy-dispersive spectrometry (EDS) of a micaceous mineral found at the Cerchiara mine, Eastern Liguria (Italy) (Fig. 1), showed a composition suggesting a new Mn-rich member of the mica group. The analyses indicated a very high Si, Mn and Mg content, with rather high F and low Al and Fe concentrations. Therefore, the mineral under investigation was considered interesting enough to proceed with additional examinations.

This paper describes the results of a chemical, structural and spectroscopic study to define and describe this new mica, named manganiceladonite from 'celadonite' and 'mangani', in allusion to the dominant Mn^{3+} trivalent octahedral cation instead of Fe^{3+}. The mineral and its name have been approved by the Commission on New Minerals, Nomenclature and Classification of the International Mineralogical Association (IMA 2015-052). The holotype material is deposited in the mineralogical collections of the Museo di Storia Naturale, Università di Firenze (Italy), under catalogue number 3164/I.

Occurrence and physical properties

Manganiceladonite was found in the metacherts of the ophiolitic sequences at Cerchiara mine, Val di Vara, Eastern Liguria, Italy (~44°11′58″N; 9°42′1″E). Since then, studies of the Cerchiara ores have led to the description of many new minerals: mozartite (Basso *et al*., 1993), brewsterite-(Ba) (Cabella *et al*., 1993), caoxite (Basso *et al*., 1997), cerchiaraite-(Mn) (Basso *et al*., 2000), cerchiaraite-(Fe) (Kampf *et al*., 2013) and balestraite (Lepore *et al*., 2015). According to Cabella *et al*. (1998), the ore body of the Cerchiara mine consists of braunite with minor quartz layers interbedded with hematite and quartz bands originated at low-temperature metamorphic conditions. The ore was produced by precipitation from submarine hydrothermal vents and reworked by turbiditic resedimentation. Manganiceladonite is orange-brown in colour with a micaceous appearance and forms thin and extremely elongated lamellae in radial aggregates associated with calcite, hematite and braunite. The lamellae are so elongated to resemble, at a glance, acicular crystals. The mineral is transparent with silky lustre and perfect {001} cleavage. It is moderately pleochroic, from orange to greenish yellow. Calculated density is 3.042 g/cm^3 on the basis of the empirical formula and unit-cell dimensions determined from powder X-ray diffraction data (see below).

FIG. 1. Manganiceladonite associated with calcite and braunite (L. Ceccantini photo); field of view is 2 mm.

Experimental details

Powder X-ray diffraction

Numerous attempts to perform single-crystal X-ray analysis were unsuccessful. Therefore, several minute fragments were handpicked from the rock sample and crushed under acetone. Given the paucity of material, it was possible to retrieve only a small amount of powder, which was not enough to allow for a sample preparation suitable for preventing preferred orientation. The spectrum was measured over the range 8 < 2θ <70° using a Bruker D8-Advance diffractometer

TABLE 1. Observed and calculated *d* spacings.

h k l	$d_{(obs)}$	$d_{(calc)}$	I/I_0
0 0 1	10.06	10.078	100
0 0 2	5.03	5.039	8
0 2 0	4.482	4.458	6
0 2 1	4.091	4.077	4
0 0 3	3.359	3.359	60
0 2 2	3.328	3.339	49
1 1 2	3.034	3.045	19
0 2 3	2.686	2.683	6
0 0 4	2.517	2.519	6
$\bar{2}$ 2 3	2.015	2.011	15
0 4 4	1.679	1.669	5
$\bar{1}$ 5 4	1.439	1.445	6

https://doi.org/10.1180/minmag.2016.080.087 Published online by Cambridge University Press

with 'Da Vinci' design equipped with Cu$K\alpha$ radiation, θ-θ goniometer and a multichannel fast detector. Background was removed by using standard polynomials through the software *Rex.Cell* (Bortolotti and Lonardelli, 2013). Determination of peak positions was carried out initially in *Rex.Cell* by means of an automated filtering/second-derivative approach based on the Savitzky–Golay method (Savitzky and Golay, 1964) and then carefully checked for incorrectly added peaks. Resulting *d* spacings are shown in Table 1.

Transmission electron microscopy

Transmission electron microscopy (TEM) was performed with a JEOL 2010 microscope, working at 200 kV and equipped with a LaB_6 electron source, ultra-high resolution (UHR) pole pieces and an Oxford ISIS energy dispersive X-ray (EDX) detector. Images (Fig. 2) and diffraction patterns were recorded with an Olympus Tengra camera (14 bit, 2048 × 2048 pixels) and analysed by 'iTEM' software. The powdered sample was dispersed on a Cu mesh. Electron diffraction tomographic (EDT) data were acquired in a tilt range of ±25° using a JEOL double tilt holder, with a SAED aperture of 20 μm (equivalent to an illuminated sample area of ~200 nm). Data analysis was performed using *ADT3D* software (Kolb *et al*., 2011).

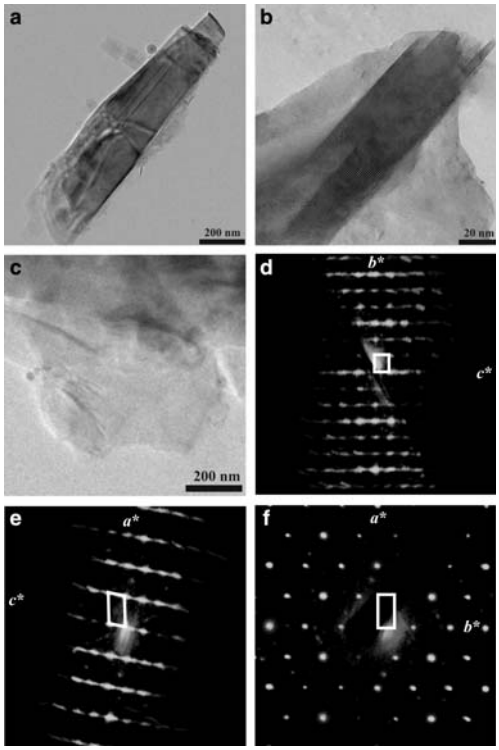

FIG. 2. (*a*) Low magnification bright field TEM image of manganiceladonite forming nanosized thin lamellae; (*b*) high-resolution TEM image of a manganiceladonite bundle viewed orthogonal to **c***; (*c*) TEM image of the crystal selected for the collection of tomographic electron diffraction data. Reconstructed three-dimensional electron diffraction volume viewed along **a*** (*d*), **b*** (*e*) and **c*** (*f*); in (*d*) and (*f*) the projections of c* and a* on (100) and (001), respectively, are shown.

Chemical analyses

A crystal aggregate of about 200 μm × 80 μm × 80 μm was embedded in epoxy and polished for electron microprobe analysis. Electron microprobe analyses were performed using a JEOL JXA-8600 instrument in wavelength dispersion mode at 15 kV, 10 nA beam current and 5 μm beam size. The following standards were used: albite (Si$K\alpha$), plagioclase (Al$K\alpha$), bustamite (Mn$K\alpha$), olivine (Mg$K\alpha$), ilmenite (Fe$K\alpha$), sanidine (K$K\alpha$), fluorite (F$K\alpha$).

Determination of Li content was carried out on the same aggregate using laser-ablation inductively-coupled-plasma mass-spectrometry (LA-ICP-MS). The laser probe consists of a Q-switched Nd:YAG laser, model Quantel (Brilliant), whose fundamental emission in the near-IR region (1064 nm) was converted into 266 nm wavelength using two harmonic generators. The spot diameter was in the range of 40–50 μm. The ablated material was analysed by using an Elan DRC-e quadrupole mass spectrometer. Helium was used as carrier gas and mixed with Ar downstream of the ablation cell. Data reduction was carried out using *Glitter* software (http://www.glitter-gemoc.com). NIST SRM 610 was analysed as an external standard, while the SiO_2 was used as an internal standard. Precision and accuracy were assessed from repeated analyses of the BCR-2 g, NIST SRM 612 and 610 standards and resulted in better than 3%. Full analytical details are reported in Tiepolo *et al*. (2005) and Miller *et al*. (2007). Chemical analyses of major elements are reported in Table 2 (means and ranges in wt.% of oxides).

Electron paramagnetic resonance (EPR) spectroscopy

Conventional continuous-wave (cw) EPR spectroscopy measurements were performed on loose sample crystals, put into amorphous silica tubes. Data were

https://doi.org/10.1180/minmag.2016.080.087 Published online by Cambridge University Press

TABLE 2. Chemical analyses (means and ranges, wt.% oxides).

Constituent	Mean	Range	SD	Probe standard
SiO_2	55.90	54.34–56.84	0.40	albite (Si*K*α)
Al_2O_3	1.20	0.37–2.66	0.05	plagioclase (Al*K*α)
Mn_2O_3	21.50	17.77–26.46	0.06	bustamite (Mn*K*α)
MgO	7.75	5.56–9.10	0.20	olivine (Mg*K*α)
Fe_2O_3	0.47	0.24–0.72	0.06	ilmenite (Fe*K*α)
K_2O	9.37	8.48–9.85	0.10	sanidine (K*K*α)
Li_2O*	0.71	0.61–0.78	0.25	NIST SRM 610
F	0.35	0.25–0.52	0.04	fluorite (F*K*α)
Total	97.25			
O≡F	0.15			
Total	97.10			
$H_2O^{\dagger}$	4.14			
Total	101.24			

Cr, V, Ti and Cl were sought but were found to be below the detection limit (<0.01 wt.%). *Measured by LA-ICP-MS. † Estimated H_2O content.

collected at room temperature, by using a Bruker ER 200D-SRC spectrometer operating at X-Band (~9.5 GHz) interfaced with DS/EPR software to a PC for data acquisition and handling. Given the extremely small amount of material available for the spectroscopic measurement, EPR spectra were collected in the range 1000–6000 G integrating 30 repeated scans registered at a scan speed of 0.1953s per gauss, for a total integrated counting time of 3.5 h. The EPR spectrum is shown in Fig. 3.

Raman spectroscopy

The Raman spectrum (Fig. 4) was obtained using a micro/macro Jobin Yvon LabRam HRVIS, equipped with a motorized *x-y* stage and an Olympus microscope. The back-scattered Raman signal was collected with 50x objective and the Raman spectrum was obtained from a non-oriented crystal (8 μm × 30 μm × 100 μm, approximately). The 632.8 nm line of a He-Ne laser was used as excitation; laser power was controlled with a series of density filters. The minimum lateral and depth resolution were ~2 and 5 μm, respectively. The system was calibrated using the 520.6 cm^{-1} Raman band of silicon before the experimental session. Spectra were collected with multiple acquisitions (2 to 6) with single counting times ranging between 20 and 180 s. The spectrum was recorded using the *LabSpec 5* program (HORIBA, Jobin Yvon, France) from 150 to 4000 cm^{-1}.

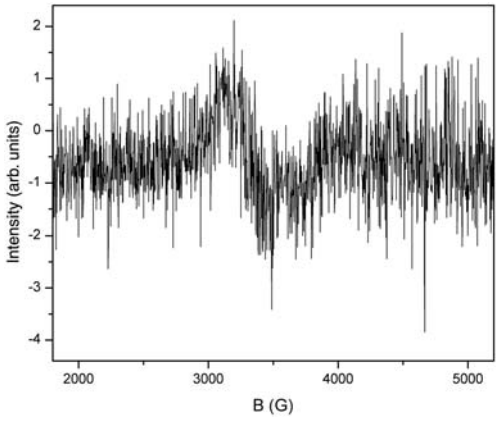

FIG. 3. Electron paramagnetic resonance spectrum of manganiceladonite.

Results and discussion

The powder X-ray diffraction pattern closely resembles that of a mica (e.g. Odom, 1984). Low magnification TEM images show that manganiceladonite preferentially crystallizes with an elongated platelet habit (Fig. 2*a*). High-resolution TEM (HRTEM) images reveal that crystals tend to fray in bended lamellae that can be as thin as 20 nm (Fig. 2*b*). This morphology explains the difficulties in finding suitable crystals for single-crystal X-ray analysis. Data from EDT were collected from the crystal shown in Fig. 2*c*. The reconstructed three-dimensional electron diffraction volume (Figs 2*d–f*) shows indeed a *C* lattice compatible with a mica

https://doi.org/10.1180/minmag.2016.080.087 Published online by Cambridge University Press

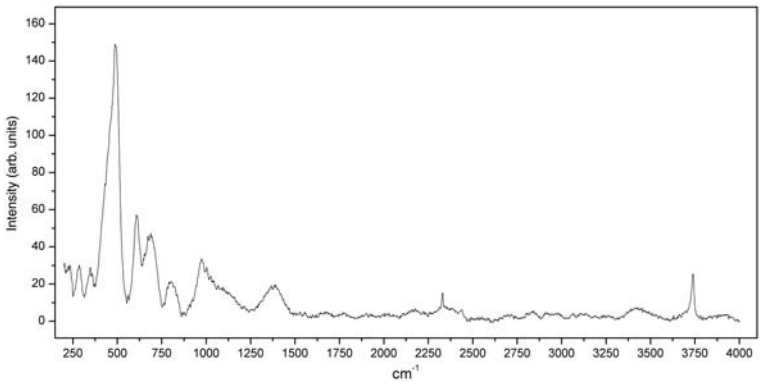

FIG. 4. Raman spectrum of manganiceladonite.

(cell parameters: a = 5.4(1) Å, b = 9.1(2) Å, c = 9.8(2) Å, β = 101.5(10)°, V = 472 Å^3). The pattern is characterized by a strong diffuse scattering along **c***, indicating strong stacking disorder along this direction.

The choice of a criterion for formula calculation, which in micas involves an arduous task requiring a direct determination of the hydrogen content, is, in this case, even more complicated due to the presence of an elevated content of Mn, which could be present at different valence states (+2, +3, +4). Manganese in micas is indeed reported commonly as Mn^{2+} although it rarely occurs at the trivalent state, such as in norrishite; in the case of manganiceladonite, given the strongly oxidizing conditions assessed at the Cerchiara mine (Lepore *et al*., 2015 and references therein), even the presence of Mn^{4+} has to be taken into account. The analysis of the EPR spectrum excludes the presence of Mn^{2+}, which would produce a characteristic six-fold feature due to hyperfine splitting. The weak paramagnetic signal observed (Fig. 3) is then attributed to the presence of Mn^{4+}. In order to obtain an evaluation of the Mn^{4+} concentration, a sample of birnessite containing 62.67 Mn (wt.%) of which 62% is considered as Mn^{4+} (Di Leo *et al.*, 2012; 2013) was used as the external standard. The spectrum was acquired under the same conditions (1000–6000 G range, 0.1953s per gauss) in a single scan. Taking into account that the intensity of the peak relative to Mn^{4+}, corrected for the differences in acquisition time and sample mass, is ~34 times higher than the peak observed for manganiceladonite, it was possible to obtain a rough estimate of Mn^{4+} content (1.1 wt.%) in this latter phase, which corresponds to ~1.8 MnO_2 (wt.%). This value can be considered as upper estimated. Nevertheless, given the impossibility to obtain an accurate quantification of the Mn^{3+}/Mn^{4+} ratio, for further calculations Mn was assumed to occur in its trivalent state, which is undoubtedly the prevalent one. In addition, the Raman spectrum (Fig. 4), although subjected to high noise level, exhibits a distinct peak in the OH stretching region (3738 cm^{-1}), indicating the presence of OH groups in the structure. In consideration of the fact that it is very common for Li-rich micas to show a partial occupancy of the M1 *trans* site, it would be unfeasible to normalize the formula on the basis of a fixed number of cations. Chemical data were thus tentatively normalized assuming 22 and 23 negative charges to take into account for a fully and partially hydrogenated O4 site, respectively. As the normalization based on 23 negative charges leads to an unsatisfactory excess of tetrahedral cations (Si = 4.07; Al = 0.10 apfu), we assumed the following empirical formula, based on 22 negative charges, as the most appropriate:

$$(K_{0.83}\square_{0.17})(Mn^{3+}_{1.14}Mg_{0.80}Li_{0.20}Fe^{3+}_{0.02})_{\Sigma=2.16}$$
$$(Si_{3.89}Al_{0.10})_{\Sigma=3.99}O_{10}[(OH)_{1.92}F_{0.08}].$$

Tetrahedral sites in manganiceladonite are almost fully occupied by Si and octahedra are filled by Mn^{3+} and Mg, with a sum close to the typical value of a dioctahedral mica; Li has been attributed to the octahedral sites, as it is reported commonly in the literature (e.g. Brigatti *et al*., 2002). The corresponding ideal end-member formula is then $KMn^{3+}MgSi_4O_{10}(OH)_2$ which is related to celadonite by the homovalent substitution $^{VI}Mn^{3+} \rightarrow {}^{VI}Fe^{3+}$. In accordance with this conclusion, d values calculated from fitted peak positions in the X-ray spectrum (Table 1) were used to refine the unit-cell

https://doi.org/10.1180/minmag.2016.080.087 Published online by Cambridge University Press

parameters using the software *UnitCell* (Holland and Redfern, 1997), basing the assignment of *hkl* reflection positions on the data from Zhukhlistov (2005) for celadonite-1*M*. The resulting monoclinic cell is: $a = 5.149(1)$, $b = 8.915(1)$, $c = 10.304(1)$ Å, $\beta = 102.03(1)°$. Measured and calculated *d* values are compared in Table 1. In analogy with the ideal crystal structure of mica and, specifically, with that of celadonite, we can assume that the most likely space groups are *C*2 or *C*2/*m*, and the polytype 1*M*. The small *b* value is consistent with that of a dioctahedral mica, in agreement with chemical data.

The 'transitional' character of manganiceladonite is a common feature, especially for Li-bearing micas (e.g. Levinson, 1953; Černý *et al*., 1995; Roda-Robles *et al*., 2006; Van Lichtervelde *et al*. 2008; Martins *et al*., 2012). The experimental work of Monier and Robert (1986) also showed how the gap between dioctahedral and trioctahedral micas reduces with a progressive increase in Li. Du Bray (1994) and Foord *et al*. (1995) also suggested that the intermediate occupancy of the octahedral sheet could be indicative of a mixed-layer form, involving both dioctahedral and trioctahedral structures, and could be a sign of disequilibrium crystallization. The sum of interlayer cations <0.90 apfu constitutes an unusual feature in the mica-group chemistry; nonetheless, micas from metamorphic environments commonly show interlayer sites not fully occupied (e.g. Brigatti *et al*., 2011); moreover the presence of a minor amount of Li in the interlayer cavity can also be hypothesized (Robert *et al*., 1983; Mesto *et al*., 2006), but cannot be verified in the absence of a structure refinement.

Acknowledgements

The manuscript benefited from the revisions of two anonymous reviewers and the editorial handling of Sergey V. Krivovichev. The authors also thank Massimo Batoni for providing the sample and Luca Ceccantini for the photo of manganiceladonite. The X-ray diffraction spectrum was measured at CRIST, Centro di Cristallografia Strutturale, University of Florence, Italy. EDT measurements were supported by FIR2013-Exploring the Nanoworld. This work was funded by "Progetto d'Ateneo 2013" to P. Bonazzi and F. Di Benedetto.

References

Basso, R., Lucchetti, G., Zefiro, L. and Palenzona, A. (1993) Mozartite, $CaMn(OH)SiO_4$, a new mineral species from the Cerchiara mine, northern Apennines, Italy. *The Canadian Mineralogist*, **31**, 331–336.

Basso, R., Lucchetti, G., Zefiro, L. and Palenzona, A. (1997) Caoxite, $Ca(H_2O)_3(C_2O_4)$, a new mineral from the Cerchiara mine, northern Appennines, Italy. *Neues Jahrbuch für Mineralogie, Monatshefte*, 84–96.

Basso, R., Lucchetti, G., Zefiro, L. and Palenzona, A. (2000) Cerchiaraite, a new natural Ba-Mn-mixedanion silicate chloride from the Cerchiara mine, northern Apennines, Italy. *Neues Jahrbuch für Mineralogie, Monatshefte*, 373–384.

Boggs, R.C. (1992) A manganese-rich miarolitic granite pegmatite assemblage from the Sawtooth batholith, South central Idaho, U.S.A. *Abstracts: International Symposium "Lepidolite 200", Nové Město na Moravě/ Czechoslovakia*, 29.8.-3.9.1992, 15–16.

Bortolotti, M. and Lonardelli, I. (2013) ReX. Cell: a user-friendly program for powder diffraction indexing. *Journal of Applied Crystallography*, **46**, 259–261.

Brigatti, M.F. and Guggenheim, S. (2002) Mica crystal chemistry and the influence of pressure, temperature, and solid solution on atomistic models. Pp. 1–97 in: *Micas: Crystal Chemistry & Metamorphic Petrology* (A. Mottana, F.P. Sassi, J.B. Thompson, Jr. and S. Guggenheim, editors). Reviews in Mineralogy and Geochemistry, **46**. Mineralogical Society of America and the Geochemical Society, Chantilly, Virginia, USA.

Brigatti, M.F., Malferrari, D., Laurora, A. and Elmi, C. (2011) Structure and mineralogy of layer silicates: recent perspectives and new trends. Layered mineral structures and their application in advanced technologies. *EMU Notes in Mineralogy*, **11**, 1–71.

Cabella, R., Lucchetti, G., Palenzona, A., Quartieri, S. and Vezzalini, G. (1993) First occurrence of a Ba-dominant brewsterite: structural features. *European Journal of Mineralogy*, **5**, 353–360.

Cabella, R., Lucchetti, G. and Marescotti, P. (1998) Mn-ores from Eastern Ligurian ophioltic sequences ("Diaspri di Monte Alpe" Formation, Northern Apennines, Italy). *Trends in Mineralogy*, **2**, 1–17.

Černý, P., Chapman, R., Staně, J., Nová, M., Baadsgaard, H., Rieder, M., Kavalová, M. and Ottolini, L. (1995) Geochemical and structural evolution of micas in the Rožná and Dobrá Voda pegmatites, Czech Republic. *Mineralogy and Petrology*, **55**, 177–201.

Di Leo, P., Pizzigallo, M.D.R., Ancona, V., Di Benedetto, F., Mesto, E., Schingaro, E. and Ventruti, G. (2012) Mechanochemical transformation of an organic ligand on mineral surfaces: The efficiency of birnessite in catechol degradation. *Journal of Hazardous Materials*, **201**, 148–154.

Di Leo, P., Pizzigallo, M.D.R., Ancona, V., Di Benedetto, F., Mesto, E., Schingaro, E. and Ventruti, G. (2013) Mechanochemical degradation of pentachlorophenol onto birnessite. *Journal of Hazardous Materials*, **244**, 303–310.

https://doi.org/10.1180/minmag.2016.080.087 Published online by Cambridge University Press

Du Bray, E.A. (1994) Compositions of micas in peraluminous granitoids of the eastern Arabian Shield. *Contributions to Mineralogy and Petrology*, **116**, 381–397.

Eggleton, R.A. and Ashley, P.M. (1989) Norrishite, a new manganese mica, $K(Mn_2^{3+}Li)\ Si_4O_{12}$, from the Hoskins Mine, New South Wales, Australia. *American Mineralogist*, **74**, 1360–1367.

Foord, E.E., Černý, P., Jackson, L.L., Sherman, D.M. and Eby, R.K. (1995) Mineralogical and geochemical evolution of micas from miarolitic pegmatites of the anorogenic Pikes Peak batholith, Colorado. *Mineralogy and Petrology*, **55**, 1–26.

Guggenheim, S., Schulze, W.A., Harris, G.A. and Lin, J. C. (1983) Concentric layer silicates: An optical second harmonic generation, chemical and X-ray study. *Clays and Clay Minerals*, **31**, 251–260.

Harada, K., Honda, M., Nagashima, K. and Kanisawa, S. (1976) Masutomilite, manganese analogue of zinnwaldite, with special reference to masutomilite–lepidolite–zinnwaldite series. *Mineralogical Journal*, **8**, 95–109.

Holland, T.J.B. and Redfern, S.A.T. (1997) UNITCELL: a nonlinear least-squares program for cell-parameter refinement and implementing regression and deletion diagnostics. *Journal of Applied Crystallography*, **30**, 84–84.

Ishida, K., Hawthorne, F.C. and Hirowatari, F. (2004) Shirozulite, $KMn_3^{2+}(Si_3Al)O_{10}(OH)_2$, a new manganese-dominant trioctahedral mica: Description and crystal structure. *American Mineralogist*, **89**, 232–238.

Kampf, A.R., Roberts, A.C., Venance, K.E., Carbone, C., Belmonte, D., Dunning, G.E. and Walstrom, R.E. (2013) Cerchiaraite-(Fe) and cerchiaraite-(Al), two new barium cyclosilicate chlorides from Italy and California, USA. *Mineralogical Magazine*, **77**, 69–80.

Kolb, U., Mugnaioli, E. and Gorelik, T.E. (2011) Automated electron diffraction tomography – a new tool for nano crystal structure analysis. *Crystal Research and Technology*, **46**, 542–554.

Lepore, G.O., Bindi, L., Zanetti, A., Ciriotti, M., Medenbach, O. and Bonazzi, P. (2015) Balestraite, $KLi_2VSi_4O_{10}O_2$, the first member of the mica group with octahedral V^{5+}. *American Mineralogist*, **100**, 608–614.

Levinson, A.A. (1953) Studies in the mica group; relationship between polymorphism and composition in the muscovite-lepidolite series. *American Mineralogist*, **38**, 88–107.

Martins, T., Roda-Robles, E., Lima, A. and de Parseval, P. (2012) Geochemistry and evolution of micas in the Barroso–Alvão pegmatite field, Northern Portugal. *The Canadian Mineralogist*, **50**, 1117–1129.

Mesto, E., Schingaro, E., Scordari, F. and Ottolini, L. (2006) An electron microprobe analysis, secondary ion mass spectrometry, and single crystal X-ray diffraction study of phlogopites from Mt. Vulture, Potenza, Italy: Consideration of cation partitioning. *American Mineralogist*, **91**, 182–190.

Miller, C., Zanetti, A., Thöni, M. and Konzett, J. (2007) Trace element mineral chemistry of the type locality (Koralpe, Saualpe) and Pohorje eclogites (Eastern Alps): implications for behaviour of fluid-mobile elements in a continental subduction zone, geochronology and geothermometry. *Chemical Geology*, **239**, 96–123.

Monier, G. and Robert, J.L. (1986) Evolution of the miscibility gap between muscovite and biotite solid solutions with increasing lithium content: an experimental study in the system $K_2O–Li_2O–MgO–FeO–Al_2O_3–SiO_2–H_2O–HF$. *Mineralogical Magazine*, **50**, 641–651.

Odom, I.E. (1984) Glauconite and celadonite minerals. Pp. 545–572 in: *Micas* (S.W. Bailey, editor). Reviews in Mineralogy and Geochemistry, **13**. Mineralogical Society of America, Washington, DC.

Robert, J.L. and Maury, R.C. (1979) Natural occurrence of a (Fe, Mn, Mg) tetrasilicic potassium mica. *Contributions to Mineralogy and Petrology*, **68**, 117–123.

Robert, J.L., Volfinger, M., Barrandon, J.N. and Basutçu, M. (1983) Lithium in the interlayer space of synthetic trioctahedral micas. *Chemical Geology*, **40**, 337–351.

Roda-Robles, E., Pesquera, A., Gil-Crespo, P.P., Torres-Ruiz, J. and De Parseval, P. (2006) Mineralogy and geochemistry of micas from the Pinilla de Fermoselle pegmatite (Zamora, Spain). *European Journal of Mineralogy*, **18**, 369–377.

Savitzky, A. and Golay, M.J. (1964) Smoothing and differentiation of data by simplified least squares procedures. *Analytical Chemistry*, **36**, 1627–1639.

Tiepolo, M., Zanetti, A. and Vannucci, R. (2005) Determination of Li, Be and B at trace levels by LA-ICP-MS. *Geostandards and Geoanalytical Research*, **29**, 211–224.

Tischendorf, G., Förster, H.J., Gottesmann, B. and Rieder, M. (2007) True and brittle micas: composition and solid-solution series. *Mineralogical Magazine*, **71**, 285–320.

Tracy, R.J. and Beard, J.S. (2003) Manganoan kinoshitalite in Mn-rich marble and skarn from Virginia. *American Mineralogist*, **88**, 740–747.

Tyrna, P.L. and Guggenheim, S. (1991) The crystal structure of norrishite, $KLiMn_2^{3+}Si_4O_{12}$: an oxygen-rich mica. *American Mineralogist*, **76**, 266–271.

Van Lichtervelde, M., Grégoire, M., Linnen, R.L., Béziat, D. and Salvi, S. (2008) Trace element geochemistry by laser ablation ICP-MS of micas associated with Ta mineralization in the Tanco pegmatite, Manitoba, Canada. *Contributions to Mineralogy and Petrology*, **155**, 791–806.

Zhukhlistov, A.P. (2005) Crystal structure of celadonite from the electron diffraction data. *Crystallography Reports*, **50**, 902–906.

https://doi.org/10.1180/minmag.2016.080.087 Published online by Cambridge University Press